Biomedical Optics EXPRESS

Fourier phase microscopy with white light

Basanta Bhaduri,[1] Krishnarao Tangella,[2] and Gabriel Popescu[1,*]

[1]*Quantitative Light Imaging Laboratory, Department of Electrical and Computer Engineering, University of Illinois at Urbana-Champaign, Urbana, IL 61801, USA*

[2]*Christie Clinic and University of Illinois at Urbana-Champaign, Department of Pathology 1400 West Park Street, Urbana, Illinois 61801, USA*

[*]*gpopescu@illinois.edu*

Abstract: Laser-based Fourier phase microscopy (FPM) works on the principle of decomposition of an image field in two spatial components that can be controllably shifted in phase with respect to each other. However, due to the coherent illumination, the contrast in phase images is degraded by speckles. In this paper we present FPM with spatially coherent white light (wFPM), which offers high spatial phase sensitivity due to the low temporal coherence and high temporal phase stability due to common path geometry. Further, by using a fast spatial light modulator (SLM) and a fast scientific-grade complementary metal oxide semiconductor (sCMOS) camera, we report imaging at a maximum rate of 12.5 quantitative phase frames per second with 5.5 mega pixels image size. We illustrate the utility of wFPM as a contrast enhancement as well as dynamic phase measurement method by imaging section of benign colonic glands and red blood cell membrane fluctuation.

OCIS codes: (170.0180) Microscopy; (070.0070) Fourier optics and signal processing; (070.6120) Spatial light modulators; (120.5050) Phase measurement.

References and links

1. E. Abbe, "Beiträge zur Theorie des Mikroskops und der mikroskopischen Wahrnehmung," Archiv Für Mikroskopische Anatomie **9**, 431–468 (1873).
2. G. Popescu, *Quantitative phase imaging of cells and tissues* (McGraw-Hill, New York, 2011).
3. P. Marquet, B. Rappaz, P. J. Magistretti, E. Cuche, Y. Emery, T. Colomb, and C. Depeursinge, "Digital holographic microscopy: A noninvasive contrast imaging technique allowing quantitative visualization of living cells with subwavelength axial accuracy," Opt. Lett. **30**(5), 468–470 (2005).
4. T. Ikeda, G. Popescu, R. R. Dasari, and M. S. Feld, "Hilbert phase microscopy for investigating fast dynamics in transparent systems," Opt. Lett. **30**(10), 1165–1167 (2005).
5. C. J. Mann, L. Yu, C.-M. Lo, and M. K. Kim, "High-resolution quantitative phase-contrast microscopy by digital holography," Opt. Express **13**(22), 8693–8698 (2005).
6. G. Popescu, T. Ikeda, R. R. Dasari, and M. S. Feld, "Diffraction phase microscopy for quantifying cell structure and dynamics," Opt. Lett. **31**(6), 775–777 (2006).
7. N. T. Shaked, J. D. Finan, F. Guilak, and A. Wax, "Quantitative phase microscopy of articular chondrocyte dynamics by wide-field digital interferometry," J. Biomed. Opt. **15**(1), 010505 (2010).
8. D. Zicha, E. Genot, G. A. Dunn, and I. M. Kramer, "TGFbeta1 induces a cell-cycle-dependent increase in motility of epithelial cells," J. Cell Sci. **112**(Pt 4), 447–454 (1999).
9. G. Popescu, L. P. Deflores, J. C. Vaughan, K. Badizadegan, H. Iwai, R. R. Dasari, and M. S. Feld, "Fourier phase microscopy for investigation of biological structures and dynamics," Opt. Lett. **29**(21), 2503–2505 (2004).
10. N. Lue, W. Choi, G. Popescu, T. Ikeda, R. R. Dasari, K. Badizadegan, and M. S. Feld, "Quantitative phase imaging of live cells using fast Fourier phase microscopy," Appl. Opt. **46**(10), 1836–1842 (2007).
11. Z. Wang, L. Millet, M. Mir, H. F. Ding, S. Unarunotai, J. A. Rogers, M. U. Gillette, and G. Popescu, "Spatial light interference microscopy (SLIM)," Opt. Express **19**(2), 1016–1026 (2011).
12. B. Bhaduri, D. Wickland, R. Wang, V. Chan, R. Bashir, and G. Popescu, "Cardiomyocyte Imaging Using Real-Time Spatial Light Interference Microscopy (SLIM)," PLoS ONE **8**(2), e56930 (2013), http://www.plosone.org/article/info%3Adoi%2F10.1371%2Fjournal.pone.0056930.
13. K. Creath and G. Goldstein, "Dynamic quantitative phase imaging for biological objects using a pixelated phase mask," Biomed. Opt. Express **3**(11), 2866–2880 (2012).
14. B. Bhaduri, H. Pham, M. Mir, and G. Popescu, "Diffraction phase microscopy with white light," Opt. Lett. **37**(6), 1094–1096 (2012).

#190929 - $15.00 USD Received 31 May 2013; revised 21 Jul 2013; accepted 22 Jul 2013; published 25 Jul 2013

15. P. Bon, G. Maucort, B. Wattellier, and S. Monneret, "Quadriwave lateral shearing interferometry for quantitative phase microscopy of living cells," Opt. Express **17**(15), 13080–13094 (2009).
16. A. B. Parthasarathy, K. K. Chu, T. N. Ford, and J. Mertz, "Quantitative phase imaging using a partitioned detection aperture," Opt. Lett. **37**(19), 4062–4064 (2012).
17. B. Fowler, C. Liu, S. Mims, J. Balicki, W. Li, H. Do, J. Appelbaum, and P. Vu, "A 5.5Mpixel 100 Frames/sec wide dynamic range low noise CMOS Image sensor for scientific applications," Proc. SPIE **7536**, 753607 (2010).
18. http://refractiveindex.info
19. Y. K. Park, C. A. Best, K. Badizadegan, R. R. Dasari, M. S. Feld, T. Kuriabova, M. L. Henle, A. J. Levine, and G. Popescu, "Measurement of red blood cell mechanics during morphological changes," Proc. Natl. Acad. Sci. U.S.A. **107**(15), 6731–6736 (2010).
20. Y. K. Park, C. A. Best, T. Auth, N. S. Gov, S. A. Safran, G. Popescu, S. Suresh, and M. S. Feld, "Metabolic remodeling of the human red blood cell membrane," Proc. Natl. Acad. Sci. U.S.A. **107**(4), 1289–1294 (2010).
21. M. Mir, H. Ding, Z. Wang, J. Reedy, K. Tangella, and G. Popescu, "Blood screening using diffraction phase cytometry," J. Biomed. Opt. **15**(2), 027016 (2010).

1. Introduction

Optically thin specimens, including live cells, generally do not absorb or scatter light significantly, i.e., they are transparent, or phase objects. Microscopic images of these specimens are formed as a result of the interference between the scattered and unscattered fields as formulated by Abbe [1]. In quantitative phase imaging (QPI), we map nanometer scale optical path-length shifts associated with the specimen via interferometric experiments [2]. Most of the QPI methods are either *off-axis* [3–7], or *phase shifting* [8–12] based. The fastest acquisition rates are allowed by off-axis methods, because the phase information is extracted from a single recorded interferogram. On the other hand, the diffraction limited transverse resolution is intrinsically preserved in phase shifting methods. Further, pixelated phase mask has been employed recently to simultaneously record multiple phase shifted images using the polarization properties of light [13]. In QPI, we are also interested to have the highest *temporal phase sensitivity* (that is, smallest frame-to-frame phase shift), which is provided by common-path methods because they are the most stable [2]. Finally, reduction in speckles insures high spatial sensitivity. Speckles average out as the spatiotemporal coherence of light is reduced. However, since in QPI we employ spatially coherent light, use of white light to provide limited temporal coherence is the remaining option for enhancing spatial sensitivity [see, e.g., Chap. 8 in Ref. 2, for an analysis of the QPI figures of merit].

Fourier phase microscopy (FPM) is a common-path, phase shifting QPI method [9]. By use of the Fourier decomposition of optical image field into two spatial components and controllably shifting in phase with respect to each other, high-transverse-resolution QPI is generated. A 100 times faster version was also developed which is referred to as fast Fourier phase microscope (f-FPM) [10]. However, FPM and most of the other QPI methods use temporally coherent (laser) illumination and, hence, the contrast in phase images is degraded by speckles. Using broadband illumination increases the spatial sensitivity of QPI.

Recently, we have achieved this by using white light illumination in phase-shifting-based spatial light interference microscopy (SLIM) [11,12] and off-axis-based white-light diffraction phase microscopy (wDPM) [14]. Both SLIM and wDPM produce highly sensitive (both spatially and temporally) phase images. However, SLIM requires specialized phase contrast illumination and objectives. On the other hand, wDPM generates QPI with lower space-bandwidth product, i.e., it can only preserve the resolution at the expense of field of view. Quadriwave lateral shearing interferometry (QWLSI) was also proposed which is a single shot white light based method [15]. However, it doesn't measure the phase, rather phase derivative with respect to X or Y. This gradient image is further integrated to obtain the phase map, which requires assumptions about the constant of the integration [16].

In this paper we report the implementation of FPM with white-light (wFPM), which is capable of providing in real time quantitative phase images at 12.5 frames per second, with high transverse resolution, high spatial and temporal sensitivity. This performance was achieved by combining a fast spatial light modulator (SLM, Boulder Nonlinear Systems) and a fast scientific-grade complementary metal oxide semiconductor (sCMOS) camera (Neo,

#190929 - $15.00 USD Received 31 May 2013; revised 21 Jul 2013; accepted 22 Jul 2013; published 25 Jul 2013

Andor). Further, using novel software developed in house, we perform the phase reconstruction and display the quantitative phase images in real time.

2. White-light Fourier phase microscopy (wFPM)

2.1 Experimental setup

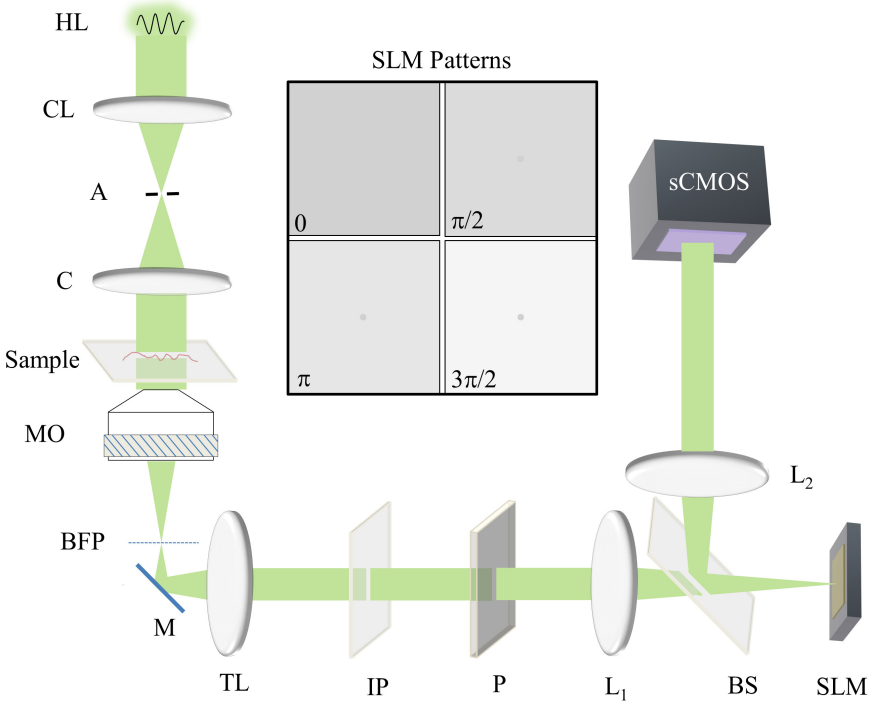

Fig. 1. Optical Set up for white-light Fourier phase microscopy (wFPM): HL, Halogen Lamp; CL, Collimating Lens; A, Aperture Stop; C, Condenser; MO, Microscope Objective; BFP, Back Focal Place; M, Mirror; TL, Tube Lens; IP, Image Plane; P, Polarizer; L_1-L_2, Fourier Lenses; BS, Beam Splitter; SLM, Spatial Light Modulator. Inset shows 4 phase shifted patterns in increments of π/2 displayed on the SLM.

A schematic of the wFPM setup is shown in Fig. 1. The imaging system represents a 4f, telecentric system, characterized by the fact that an ensemble of parallel rays at the input plane remains parallel at the output. wFPM is designed as an add-on module to a commercial bright-field microscope (Axio Observer Z1, Zeiss) which uses a halogen lamp as a white light source, with a spectrum centered at 550 nm [11]. We closed down the condenser to the minimum possible value (NA = 0.09) in order to make the illumination at the sample plane spatially coherent. wFPM relies on the spatial decomposition of the image field into its scattered, and un-scattered component. We introduced 4 phase shifts in increments of π/2 between these components. This modulation was achieved by displaying different phase patterns on a reflective SLM (inset in Fig. 1). The SLM is placed in the Fourier plane of this system which is conjugate to the back focal plane of the microscope objective (Zeiss, 40X, NA = 0.95). The active pattern on the SLM is calculated to precisely match the size and position of the condenser aperture, such that phase delay can be precisely controlled between the scattered and unscattered components of the image field. Four images (I_m, m = 1, 2, 3, 4) corresponding to each phase shift [(m-1)π/2] are recorded to produce a quantitative phase image that is uniquely determined. The polarizer is aligned with the active axis of the SLM, which insures that it is operating in pure phase modulation mode. Lens L_1 has a focal length f_1 = 150 mm and L_2 has f_2 = 200 mm; thus we obtain further f_2/f_1 = 4/3 magnification outside the microscope. We used a sCMOS camera (Neo, Andor) which is capable of imaging at 100

#190929 - $15.00 USD Received 31 May 2013; revised 21 Jul 2013; accepted 22 Jul 2013; published 25 Jul 2013

frames/s at full frame resolution of 5.5 megapixels [17]. However, there is always a compromise between acquisition rate and duration of investigation if one uses the built in camera buffer memory which is finite (4 GB). Further, the SLM switching time (10 ms) slows down wFPM acquisition speed to half the max available speed of the camera. With our in house developed integration software, we can image continuously at 50 frames/s, which is an order of magnitude more than our previous phase shifting rates. Further, we have recently incorporated another sCMOS camera (Zyla, Andor) in the setup (not used for the results in this work) which is capable of imaging continuously at 100 Hz at full frame with our software.

We have calibrated the SLM for the entire visible spectrum of the Halogen source to decide the relationship between SLM pixel grayscale values and the final phase delay introduced to the unscattered field. For this calibration, the SLM was placed between two polarizers (both at 45°) and its intensity reflectance was recorded by displaying uniform grayscale images from 0 to 255 (intensity modulation mode). However, the grayscale values from 198 to 245 are used for the phase modulation mode which shows a sinusoidal like pattern as shown in Fig. 2(a). From this intensity response of the SLM, we obtained its phase response via a Hilbert transform on Fig. 2(a), as shown in Fig. 2(b) (phase modulation mode).

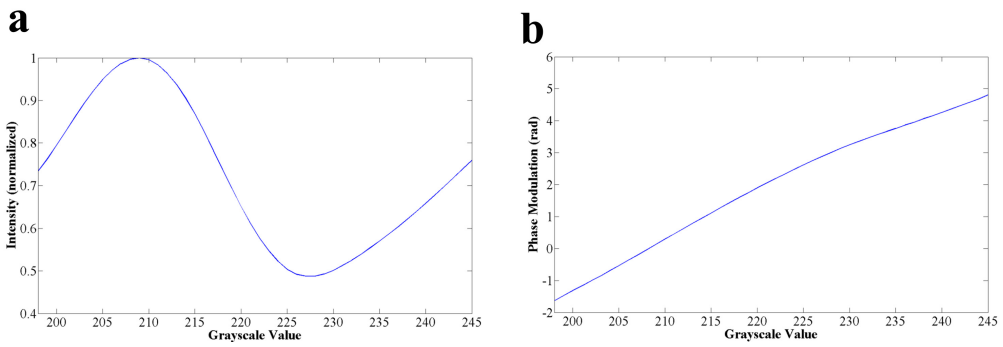

Fig. 2. SLM calibration: a) Intensity modulation obtained by displaying different grayscale values on the SLM, (b) Phase vs. grayscale calibration curve obtained by Hilbert transform of the signal in (a).

2.2 Phase retrieval

The spatially varying phase shift, $\Delta\phi$ between the scattered [$|U_1(\mathbf{r})|$] and unscattered [$U_0(\mathbf{r})$] field is obtained combining the phase shifted images as,

$$\Delta\phi(\mathbf{r}) = \arg\left[\frac{I_4(\mathbf{r}) - I_2(\mathbf{r})}{I_1(\mathbf{r}) - I_3(\mathbf{r})}\right]. \quad (1)$$

Letting β be the ratio of the scattered and unscattered field amplitudes, $\beta(\mathbf{r}) = |U_1(\mathbf{r})| / |U_0(\mathbf{r})|$, the phase associated with the image field is determined as [9]:

$$\phi(\mathbf{r}) = \arg\left[\frac{\beta(\mathbf{r})\sin(\Delta\phi(\mathbf{r}))}{1 + \beta(\mathbf{r})\cos(\Delta\phi(\mathbf{r}))}\right]. \quad (2)$$

The factor β can be obtained using the procedure described in Ref. 9. The quantity $\phi(\mathbf{r})$ is therefore uniquely determined from the four interferograms with no additional measurements. It is noteworthy to mention that the phase shift measured in our instrument is that of the cross correlation function associated with the broadband field.

#190929 - $15.00 USD Received 31 May 2013; revised 21 Jul 2013; accepted 22 Jul 2013; published 25 Jul 2013

2.3 System characterization and accuracy

In order to characterize the noise stability of the setup, we acquired 256 time lapse optical path difference (OPD) maps of size 256 x 256 pixels^2 at a particular location of a cover glass (without any sample). In order to subtract the static background of our system, we acquired a single OPD map ('reference image') of the same size at a different location of the same cover glass. Figure 3(a) shows the temporal standard deviation (STD) map (obtained by performing STD at each pixel of 256 subtracted OPD maps) which characterizes the noise distribution of the wFPM system. Figure 3(b) shows the histogram of this map, with a mean value of $\sigma = 0.4$ nm, representing the overall spatiotemporal noise of the system which is an order of magnitude lower than the noise level obtained using laser (5 nm). The Color bars in Fig. 3(a) and 3(b) show the STD in nm.

In order to determine the accuracy of the system, we imaged polystyrene beads (refractive index, 1.596 at 550 nm [18]; mean diameter, 1.92 ± 0.1 µm, as provided by the manufacturer) immersed in Zeiss immersion oil (refractive index 1.518). Figure 3(c) shows the quantitative phase image of such a bead. The color bar shows the phase in rad and the scale bar shows the size in µm. The measured height is 1.95 ± 0.1 µm which matches very well with the expected value. The dashed line in Fig. 3(d) shows the height profile of the bead in Fig. 3(c) (along the dashed line). For comparison, we have also plotted the theoretical profile of a 2 µm bead in Fig. 3(d) (dotted). Note that due to the finite resolution, the fit is not expected to be perfect.

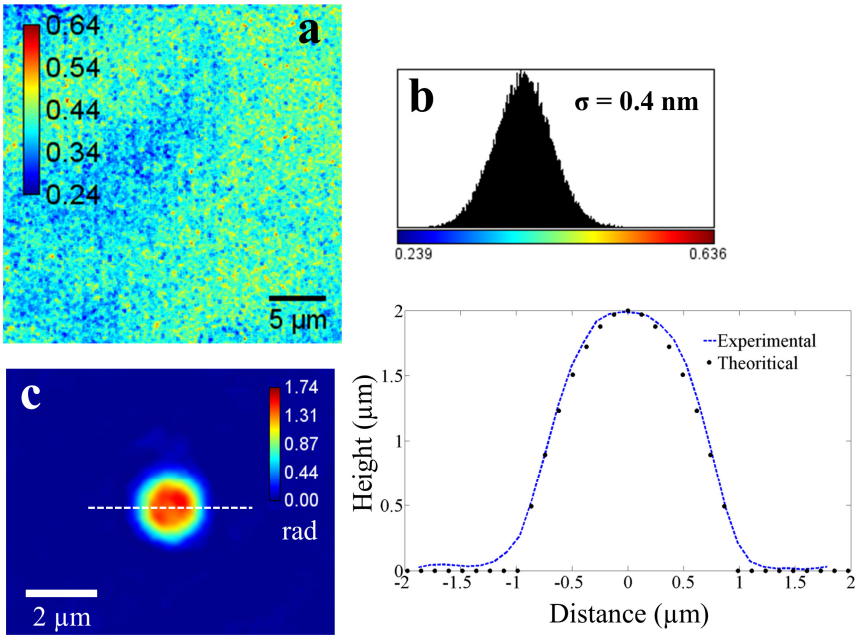

Fig. 3. wFPM System characterization and accuracy. (a) Standard deviation (STD) map of the 256 difference images. (b) Histogram of the STD map in a). (c) QPI of 2 µm bead in oil. (d) Height profile along the dashed line in c). The dotted profile in d) shows the theoretical height profile. The Color bars in a) and b) show STD in nm and in d), phase in rad, respectively.

4. Quantitative phase imaging with wFPM

4.1 Label-free tissue sample

We first demonstrate the potential of wFPM for tissue diagnosis by imaging 3 µm section of unstained paraffin embedded benign colonic glands. Figure 4(a)-4(d) are the four phase shifted images obtained by displaying 4 different patterns on the SLM. Figure 4(e) shows the obtained quantitative phase image combining these 4 images, which also distinctly shows

#190929 - $15.00 USD Received 31 May 2013; revised 21 Jul 2013; accepted 22 Jul 2013; published 25 Jul 2013

different parts of the sample as indicated by arrows. The dark patches in Fig. 4(a)-4(d) which are due to dirt on the microscope optics, are eliminated from the phase image (Fig. 4(e)) by subtracting the background phase image obtained without any sample. The glands show a single layer of nucleus that is arranged in a systematic manner at the base of glands. No mitotic activity is observed. The glands contain abundant mucin. The lumen of the gland is small and unremarkable. The glands are surrounded by stroma which shows delicate capillaries with red blood cells. The stroma as well as stromal cells are admixed with scattered plasma cells. In order to compare, we also imaged simultaneously obtained (slightly shifted) section with hematoxylin and eosin (H&E) staining, shown in Fig. 4(f). Figure 4(e) mirrors the histological features described on the H&E stained image. The tissue sectioning was performed in a clinical lab by professional staff. There may be variation in the thickness from slice to slice; however, the thickness variation within the field of view in each slice can be assumed constant. Thus, the tissue phase image is a map of the refractive index. The red blood cells in the blood vessel as well as the cell membranes between the individual enterocytes show high refractive index. On the other hand, the mucin within the glands and lymphocytes show lower refractive index.

It is noteworthy to mention that wFPM system can be used for contrast enhancement as well. It can be seen that Fig. 4(a) which is the bright-field image (without any modulation), hardly shows any contrast. By using ± π/2 phase modulation (Fig. 4(b) and 4(d), respectively), the contrast is improved a lot where we can see individual glands. Thus by using external phase modulation we can achieve high contrast microscopic image without the need for specialized optics necessary in phase contrast or DIC microscopy.

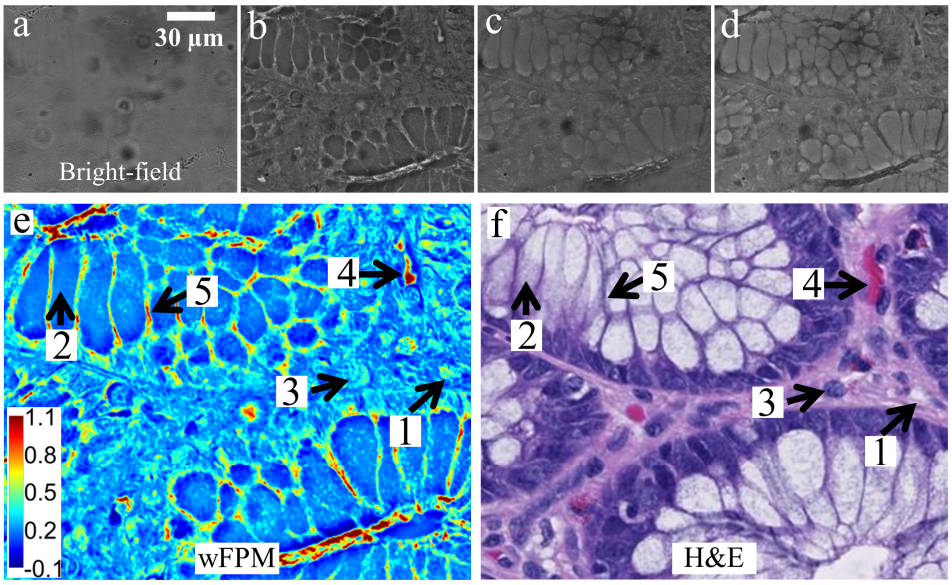

Fig. 4. Quantitative phase imaging with wFPM. Phase shifted images of section of benign colonic glands: (a) 0, (b) π/2, (c) π and (d) 3π/2, (e) phase image and (f) H&E stained image. The color bar shows the phase in radian. Arrows show different portions of the colon: arrow 1, inter-glandular stroma; arrow 2, enterocyte cytoplasm showing mucin collection; arrow 3, lymphocyte present in inter-glandular stroma; arrow 4, red blood cells in blood vessels; arrow 5, inter-cellular membrane between enterocytes.

4.2 Red blood cell membrane fluctuation

Next we imaged membrane fluctuations of red blood cells (RBC). Previously, it was found that the membrane fluctuations in the RBC have a metabolic as well as thermal energy component [19,20], which report on cell function. Prior to imaging, we centrifuged the whole blood (0.2 mL) at 1500 x g for 5 mins and then aspirated the plasma and added 1 mL of 0.1%

#190929 - $15.00 USD Received 31 May 2013; revised 21 Jul 2013; accepted 22 Jul 2013; published 25 Jul 2013

Albumin in phosphate buffer solution (PBS-A). After mixing them using a pipette, we centrifuged again at 700 x g for 5 mins and aspirated PBS-A solution to wash the RBCs. Finally we took minimal amount of blood, and added to 1 mL of PBS-A solution to make the suspension. A sample chamber is created by punching a hole in double sided scotch tape and sticking one side of the tape onto a cover slip. The suspension is then pipetted into the chamber created by the hole and it is sealed on the top using poly-L-lysine coated cover slip. The whole slide is then flipped to allow the cells to settle for 30 minutes on the coated cover slip prior to measurement. This is necessary to fix the in-plane motion of the cells. Figure 5(a) shows a 50 x 50 μm^2 size quantitative height map of live blood cells, where the normal, discocyte shape can be observed; the color bar shows the cell thickness in µm. While converting phase map into height map, we have used the refractive increment (RBC in PBS-Albumin solution), dn = 0.002 x MCHC = 0.0686, where MCHC = 34.3 g/dl, the mean cell hemoglobin concentration (provided by hospital), in the equation, $h = \lambda\phi/(2\pi\, dn)$, where λ = 550 nm, the mean wavelength of the white light [21].

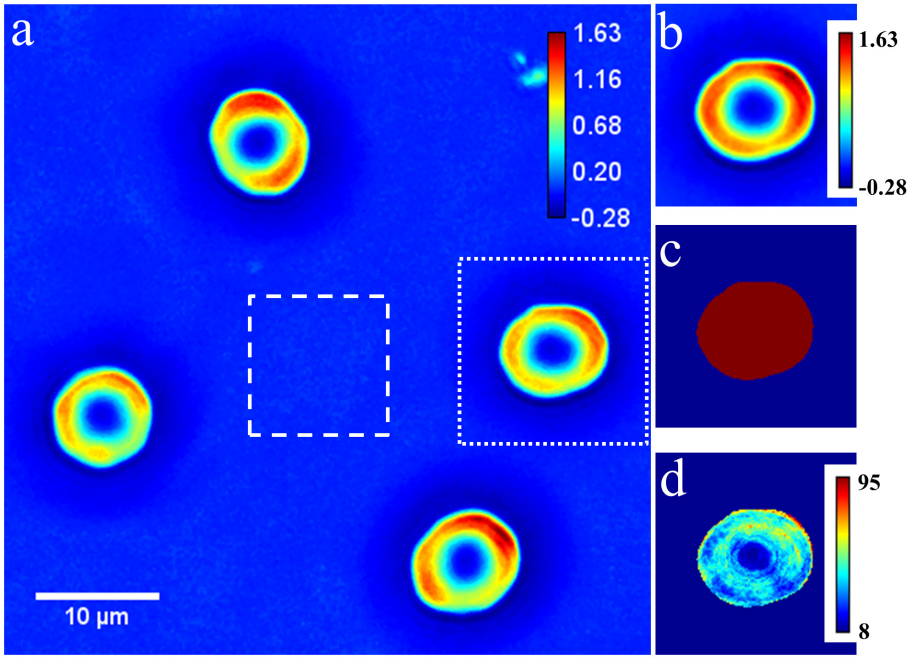

Fig. 5. Red blood cell membrane dynamics study in wFPM. (a) Quantitative phase image of RBCs. (b) Average height of the RBC shown as dotted box in a). (c) Generated mask. (d) Standard deviation of the height. The color bars in a) and b) show the cell height in µm and in d) show the standard deviation in nm, respectively.

In order to calculate RBC membrane fluctuations, we obtained 256 such time lapse phase images at 12.5 Hz (50 intensity images per second). Figure 5(b) shows the time-averaged shape of the RBC within the dotted box in Fig. 5(a). We calculated a binary mask (Fig. 5(c)) for each cell by thresholding the time-averaged map. Further, we computed the standard deviation (STD) at each pixel and multiplication with the binary mask gives the information for each individual cell (Fig. 5(d)). The color bar in Fig. 5(d) shows the STD in nm. The median of the standard deviations at all the pixels within the masked area gives the mean membrane displacement, 36.7 nm in this case. Masking is necessary in order to avoid shift in the calculated median due to large number of background pixels. Note that, the fluctuation outside the cells (dashed box in Fig. 5(a)) is 8 nm which is $1/dn$ ~15 times larger than the calculated noise level of the system (height fluctuation as compared to OPD fluctuation in Fig. 3(a)). In order to verify whether the measured fluctuation is due to cell or random, we have also measured RBC fluctuation after fixing the cell with glutaraldehyde which gives the

#190929 - $15.00 USD Received 31 May 2013; revised 21 Jul 2013; accepted 22 Jul 2013; published 25 Jul 2013

mean fluctuation of 11 nm, close to the background fluctuation. The available field of view is 300 X 250 μm^2 with the 40X objective, which indicates that many cells can be studied simultaneously. The slightly smaller values around the cell are reminiscent of the halo effect, which is well known in phase contrast microscopy. The halo effect in our images is less significant than in typical phase contrast images. This effect can be reduced further by reducing the source size, i.e., closing the condenser aperture further, however, at the expanse of giving away illumination power. We chose the current setup that compromises well image quality and acquisition rate.

5. Summary

In summary, wFPM can produce phase images with diffraction limited transverse resolution and high spatial and temporal phase sensitivity. It has the potential for diagnosis of biological specimens without the need for staining. Further real-time measurement capability of wFPM makes it suitable for fast dynamics measurements like RBC membrane fluctuations.

Acknowledgments

We are grateful to S. Sridharan for supplying the H&E stained tissue image and to D. Wickland for developing the integration software. This research was supported by the National Science Foundation (grants CBET 08-46660 CAREER, CBET-1040462 MRI). For more information, visit http://light.ece.uiuc.edu/.

#190929 - $15.00 USD Received 31 May 2013; revised 21 Jul 2013; accepted 22 Jul 2013; published 25 Jul 2013